Fabrication of various electroless Ni–P alloy/multiwalled carbon nanotube composite films on an acrylonitrile butadiene styrene resin

Susumu Arai[a,*], Toshihiko Sato[a], Morinobu Endo[b]

[a]Department of Chemistry and Material Engineering, Faculty of Engineering, Shinshu University, 4-17-1 Wakasato, Nagano-shi, Nagano 380-8553, Japan

[b]Department of Electrical and Electronic Engineering, Faculty of Engineering, Shinshu University, 4-17-1 Wakasato, Nagano-shi, Nagano 380-8553, Japan

*Corresponding author.

E-mail address: araisun@shinshu-u.ac.jp (S. Arai).

Tel: +81-26-269-5413 Fax: +81-26-269-5432

Abstract

Ni–P alloy/multiwalled carbon nanotube (MWCNT) composite films were fabricated on acrylonitrile butadiene styrene (ABS) resin by electroless plating and their microstructures, adhesion strengths, and friction properties were investigated. Various types of MWCNTs were used. In addition, various electroless plating baths were prepared to form Ni–P alloy matrices with various phosphorus contents. To enhance the adhesion strength, the ABS resin substrate was subjected to roughening treatment. The microstructures of the composite films were examined by scanning electron microscopy and X-ray diffraction. Their adhesion strengths were measured by tensile tests. The friction properties of the composite films were investigated using the ball-on-

plate method. Ni–P alloy/MWCNT composite films containing various types of MWCNTs and with Ni–P alloy matrices having various phosphorus contents were fabricated on the ABS resin substrates by electroless deposition. The adhesion strength between the Ni–P alloy/MWCNT composite films and the ABS resin substrate was more than 1300 N cm^{-2}. The Ni–P alloy/MWCNT composite films had considerably lower friction coefficients than the Ni–P alloy films. The friction coefficients of the composite films were significantly affected by the type of MWCNTs used.

Keywords: Ni–P alloy, Multiwalled carbon nanotube, Electroless plating, Composite film, Acrylonitrile butadiene styrene resin

1. Introduction

Carbon nanotubes (CNTs) [1,2] have excellent mechanical characteristics including high tensile strengths and high elastic moduli. Therefore, research into practical applications of CNTs, including the preparation of resin/CNT, ceramic/CNT, and metal/CNT composites, has been actively pursued. Recently, metal/CNT composites have been fabricated by electrodeposition [3–8] and electroless deposition [8–16]. In previous studies of electroless CNT composite plating, electroless Ni–P alloy/multiwalled carbon nanotube (MWCNT) composite coatings were reported to have superior tribological properties [8–16]. In those studies, only 20–40-nm-diameter MWCNTs were examined. Furthermore, the effects of the size or species of MWCNTs were not reported. Electroless Ni–P alloy films are generally classified into three categories based on their phosphorus content. Low phosphorus films contain about 2–4 mass% phosphorus and have a face-centered-cubic nickel structure with relatively high crystallinities. They are ferromagnetic and have been used to provide electromagnetic shielding in electronic devices such as personal computers. Films with moderate phosphorus contents contain about 6–10 mass% phosphorus and have semi-amorphous or amorphous structures. They exhibit high wear and corrosion resistances and have been most widely used as protective films for mechanical parts. High phosphorus films contain 11–13 mass% phosphorus and have an amorphous structure. They have superior corrosion resistances and are nonmagnetic. They have thus been used as undercoatings for hard disk substrates. Therefore, the effects of the phosphorus content on the microstructures and properties of the Ni–P alloy/MWCNT composite films are not only academically interesting but they are also important for practical applications. However, few studies have investigated the effects of phosphorus content on the properties of electroless Ni–P alloy/MWCNT composite films [17]. Furthermore, only metal substrates have been used in

previous studies. Electroless plating has the significant advantage that it can be used to fabricate films not only on conductive materials, such as metals, but also on insulators, such as resins and ceramics. In this study, we fabricated electroless Ni–P alloy/MWCNT composite films containing various types of MWCNTs and with Ni–P matrices with various phosphorus contents on a resin substrate. We then evaluated their adhesion strengths and friction properties.

2. Experimental

2.1. Chemicals

Commercially available vapor-grown MWCNTs, namely vapor-grown carbon fibers (VGCFs) and vapor-grown carbon nanofibers (VGNFs) (Showa Denko Co. Ltd.), and ILJINs (Iljin Nanotec Co. Ltd.) were used in the present study. Furthermore, cut VGCFs and cut VGNFs were prepared by mechanically cutting the VGCFs and VGNFs in a blender [18]. The VGCFs, VGNFs, and ILJINs had diameters of 150 nm, 80 nm, and 15 nm, respectively. These MWCNTs were about 15 μm long. The diameters of the cut VGCFs and cut VGNFs were the same as those of the VGCFs and VGNFs (150 nm and 80 nm, respectively), whereas they were about 3–5 μm and 1–3 μm in length, respectively. These lengths were measured from micrographs obtained using a field-emission scanning electron microscope (FE-SEM; JEOL, JSM-7000F). The VGCFs and VGNFs, (and hence also the cut VGCFs and cut VGNFs) are graphitized MWCNTs (heat treated at 2800 °C in argon gas for 30 min) [19]. $NiSO_4 \cdot 6H_2O$, $C_6H_5Na_3O_7$, $(NH_4)_2SO_4$, CrO_3, $Na_2B_4O_7$, Na_3PO_4, H_2SO_4, HCl, H_2O_2 (Wako Pure Chemical Industries, Ltd.), $NaH_2PO_2 \cdot H_2O$ (Kanto Chemical Co., Ltd.), and trimethyl stearyl ammonium chloride (TMSAC, Tokyo Chemical Industry Co., Ltd.) were used in this study and were special grade reagents. Pure water

from an electrodialysis water purifier (RFP343RA, Advantec MFS, Inc.) was used in all experiments. An acrylonitrile butadiene styrene (ABS) resin plate (Mitsubishi Plastics, Inc.) was used as the substrate.

2.2. Roughening of the ABS resin substrates

Adhesion between metals and resins is generally poor. To enhance the adhesion strength between the electroless Ni–P alloy/MWCNT composite films and the ABS resin substrate, the substrates were subjected to a roughening treatment. The ABS resin substrates (3×3.3×1 cm) were degreased in alkaline solution (0.15 M $Na_2B_4O_7$ + 0.12 M Na_3PO_4 + 1×10^{-4} M TMSAC) at 60 °C for 5 min. Next, the substrates were immersed in a chromic acid solution (4 M CrO_3 + 4 M H_2SO_4) at 70 °C for 10 min to roughen the substrate surfaces. The substrates were then neutralized in a solution of 0.1 M HCl and 0.1 M H_2O_2 at 35 °C for 5 min.

2.3 Sensitization and activation of the ABS resin substrates

After the roughening process, the substrates were immersed in 1 M HCl solution at room temperature for 1 min. Next, the substrates were immersed in a 4.4×10^{-2} M $SnCl_2{\cdot}2H_2O$ + 0.12 M HCl solution at 35 °C for 5 min to absorb Sn^{2+} ions on the substrates (sensitization). The substrates were then immersed in a 5.6×10^{-4} M $PdCl_2$ + 0.12 M HCl solution at 35 °C for 5 min to form palladium catalytic nuclei on the substrates (activation).

2.4. Electroless Ni–P/CNT composite plating on the ABS resin substrate

After activation, the substrates were immersed in a 1 M HCl solution and then placed in electroless plating baths to form Ni–P alloy/MWCNT composite films on the substrates. Three electroless plating baths were used: 0.1 M $NiSO_4 \cdot 6H_2O$ + 0.5 M $C_6H_5NaO_7$ + 0.2 M $NaH_2PO_2 \cdot H_2O$ + $(NH_4)_2SO_4$ + 1×10^{-4} M TMSAC + 2 g dm^{-3} MWCNT solution (bath 1), 0.1 M $NiSO_4 \cdot 6H_2O$ + 0.2 M $C_6H_5NaO_7$ + 0.2 M $NaH_2PO_2 \cdot H_2O$ + $(NH_4)_2SO_4$ + 1×10^{-4} M TMSAC + 2 g dm^{-3} MWCNT solution (bath 2), and 0.16 M $NiSO_4 \cdot 6H_2O$ + 0.08 M $C_6H_5NaO_7$ + 0.05 M $NaH_2PO_2 \cdot H_2O$ + 1×10^{-4} M TMSAC + 2 g dm^{-3} MWCNT solution (bath 3) were used to form high phosphorus, moderate phosphorus, and low phosphorus Ni–P alloy matrices, respectively. The pH of all the baths was adjusted to 9. Electroless plating was performed with stirrer agitation at 50 °C for baths 1 and 3 and at 40 °C for bath 2.

2.5. Characterization of electroless Ni–P alloy/MWCNT composite films

The surface and cross-sectional morphologies of the composite films were observed using the FE-SEM. A cross-section polisher (JEOL, SM-09010) was used to prepare cross-sectional samples for observations. Phase identification of the films was performed by X-ray diffraction (XRD) using Cu $K\alpha_1$ radiation (Shimadzu Seisakusho, XRD-6000). The phosphorus contents of the Ni–P alloy matrices were measured by electron probe microanalysis (EPMA; Shimadzu Seisakusho EPMA1610). The thicknesses of the composite films were measured from cross-sectional SEM images of the composite films.

2.6. Adhesion strength of electroless Ni–P alloy/MWCNT composite films

The adhesion strengths between the composite films and the ABS resin substrates were evaluated using a tensile adhesion tester (Phototechnica, Romulus). A stud pin with a thermosetting adhesive on its end was attached to the sample film. The adhesive was then heated to promote heat curing, resulting in strong adhesion between the stud pin and the sample film. Heating is generally performed at 150 °C for 60 min to achieve maximum adhesion strength between the stud pin and the sample film. However, since the ABS resin substrate deformed at 150 °C, heating was performed at 100 °C for 180 min in this study. Consequently, the adhesion strength between the stud pin and the sample film was lower than the maximum adhesion strength. The adhesion test was conducted by pulling the stud pin from the sample film in the perpendicular direction. The force (adhesion force) at which the stud pin separated from the sample film was measured and divided by the contact area to give the adhesion strength. If the adhesion force between the film and the substrate is lower than that between the stud pin and the sample film, exfoliation occurs between the film and the substrate (film–substrate exfoliation mode), and the measured force represents the adhesion force between the film and the substrate. However, if the adhesion force between the film and the substrate is higher than that between the stud pin and the film, exfoliation occurs between the stud pin and the film (stud pin–film exfoliation mode). In this study, the adhesion force between the film and the substrate was found to be greater than that between the stud pin and the film.

2.7. Friction properties of electroless Ni–P alloy/MWCNT composite films

The friction coefficients of the composite films were measured using a ball-on-plate type reciprocating friction tester (Nissho Electric Works, MMS-2419). An alumina ball (6 mm in diameter, Hv = 1500) was used as the counter surface. The reciprocating friction stroke was 4

mm and the tests were conducted under a normal load of 2 N. The average sliding speed was 0.5 mm s^{-1} and the number of cycles was 50. All measurements were performed under ambient conditions without any lubricants. The friction coefficient was measured continuously during the tests using a load cell.

3. Results and discussion

Fig. 1 shows surface SEM images of the ABS resin substrate before and after the surface roughening treatment. The roughened substrate has many hollows on its surface (Fig. 1(b)). These hollows were formed by selective dissolution of butadiene in the ABS resin. These hollows impart a large surface area. Furthermore, if the hollows have complex shapes and are filled with the plating film, then the plating film becomes hooked in the hollows, making it difficult to remove and resulting in high adhesion (this is known as the anchor effect).

Fig. 2 shows the growing process of a Ni–P alloy/MWCNT composite film on a roughened ABS substrate. The MWCNTs and electroless plating bath used were the VGCFs and the high-phosphorus-content bath (bath 1), respectively. At an early stage, the hollows on the substrate are filled with the deposited Ni–P alloy (Fig. 2(b)). After 10 min, the hollows are almost completely filled and some VGCFs are incorporated in the Ni–P alloy matrix (Fig. 2(c)). The Ni–P alloy/VGCF composite film then grows autocatalytically (Fig. 2(d)). Other Ni–P alloy/MWCNT composite films grew in a similar manner on the roughened ABS resin substrates.

Fig. 3 shows surface SEM images of the Ni–P alloy/MWCNT composite films with various MWCNTs fabricated from the moderate-phosphorus-content bath (bath 2). The deposition time was 90 min. For comparison, a Ni–P alloy film without MWCNTs is also shown (Fig. 3(a)). The SEM image of the Ni–P alloy/ILJIN composite film (Fig. 3(f)) has a higher magnification than

the other SEM images, because the ILJINs were very thin so that they could not be observed at the same magnification as the other CNTs. The films were about 3 μm thick, except for the Ni–P alloy/ILJIN composite film, which was about 4 μm thick. The Ni–P alloy matrix of all these films were found to have phosphorus contents of about 8 mass%, which lies in the phosphorus content range of 6–10 mass%. Therefore, these composite films have Ni–P alloy matrices with moderate phosphorus contents (see Introduction). These moderate-phosphorus-content Ni–P alloy/MWCNT composite films are relatively smooth, except for the Ni–P alloy/ILJIN composite film. A bumpy morphology consisting of spherical deposits with 2–3 μm diameters was observed on the Ni–P alloy/ILJIN composite film. All the different MWCNTs are homogeneously distributed over the film surfaces, with no significant aggregations.

The Ni–P alloy/MWCNT composite films fabricated from the high-phosphorus-content bath (bath 1) have almost the same surface morphologies as the moderate-phosphorus-content Ni–P alloy/MWCNT composite films. The phosphorus contents in the Ni–P alloy matrices of those composite films were found to be about 12 mass%, which lies in the phosphorus content range 11–13 mass%. Therefore, these composite films have Ni–P alloy matrices with high phosphorus contents (see Introduction). Thus, high-phosphorus-content Ni–P alloy/MWCNT composite films and moderate-phosphorus-content Ni–P alloy/MWCNT composite films could be successfully fabricated on the ABS resin substrates using all the different types of MWCNTs used in this study.

On the other hand, only the Ni–P alloy/ILJIN composite film could be fabricated from the low-phosphorus-content bath (bath 3). The VGCFs, the cut VGCFs, the VGNFs, and the cut VGNFs were not incorporated in the Ni–P alloy matrix. Comparing the composition of the low phosphorus content bath with those of the high and moderate phosphorus content baths, it was

noted that no $(NH_4)_2SO_4$ is present in the low phosphorus content bath. Therefore, the existence of $(NH_4)_2SO_4$ may be related to the incorporation of MWCNTs. We intend to examine the reason for this in a future study. Fig. 4 shows surface SEM images of the Ni–P alloy/ILJIN composite film from the low-phosphorus-content bath (bath 3). For comparison, a Ni–P alloy film without MWCNTs is also shown (Figs. 4(a) and (b)). The deposition time was 120 min. The Ni–P alloy/ILJIN composite film was about 6 μm thick. ILJINs are visible on the film surface in Fig. 4. The phosphorus contents of the Ni–P matrices of the films were found to be about 3 mass%, which lies in the phosphorus content range 2–4 mass%. Therefore, the Ni–P alloy matrix of the Ni–P alloy/ILJIN composite film has a low phosphorus content (see Introduction). Thus, a low-phosphorus-content Ni–P alloy/MWCNT composite film could be fabricated on ABS resin substrates using the ILJINs.

Figs. 5(a), (b), and (c) respectively show representative XRD patterns of the high-phosphorus-content, moderate-phosphorus-content, and low-phosphorus-content electroless Ni–P alloy/MWCNT composite films on the ABS resin substrates. The XRD patterns contain no diffraction peaks assigned to MWCNTs. The diffraction peaks of the MWCNTs are considered to have very weak intensities. A broad peak assigned to face-centered-cubic nickel was observed in the XRD pattern of the high-phosphorus-content Ni–P alloy/VGCF composite film (Fig. 5(a)). This indicates that the Ni–P alloy matrices of the high-phosphorus-content Ni–P alloy/MWCNT composite films have an amorphous structure. A broad peak assigned to face-centered-cubic nickel was also observed in the XRD pattern of the moderate-phosphorus-content Ni–P alloy/ILJIN composite film (Fig. 5(b)). The peak is a little sharper than that of the high-phosphorus-content composite film. This indicates that the Ni–P alloy matrices of the moderate-phosphorus-content Ni–P alloy/MWCNT composite films have an amorphous or a semi-

crystalline structure. Relatively sharp peaks assigned to face-centered-cubic nickel were observed in the XRD pattern of the low-phosphorus-content Ni–P alloy/ILJIN composite film (Fig. 5(c)). This indicates that the Ni–P alloy matrices of the low-phosphorus-content Ni–P alloy/ILJIN composite film have relatively high crystallinities.

Fig. 6 shows representative cross-sectional SEM images of the films (Fig. 6(a): a moderate-phosphorus-content Ni–P alloy film; Fig. 6(b): a moderate phosphorus-content Ni–P alloy/VGCF composite film). The black regions in the composite film are cross sections of the VGCFs (Fig. 6(b)). The hollows on the ABS resin substrate were completely filled with the Ni–P alloy/VGCF composite film, just as they were for the Ni–P alloy films. Other Ni–P alloy/MWCNT composite films had the same boundaries with the ABS resin substrates as the moderate-phosphorus-content Ni–P alloy/VGCF composite film. Therefore, the Ni–P alloy/MWCNT composite films are expected to exhibit high adhesion strengths due to the anchor effect.

Fig. 7 shows the results of measuring the adhesion strength between the moderate-phosphorus-content Ni–P alloy/MWCNT composite films and the ABS resin substrate. Based on observation of the exfoliated area, the exfoliation mode was found to be the stud pin–film exfoliation mode for all samples. Therefore, the adhesion strengths of all the samples are higher than the values shown in Fig. 7 (2000–3000 N cm^{-2}). The exfoliation mode of the high-phosphorus-content Ni–P alloy/MWCNT composite films and the low-phosphorus-content Ni–P alloy/ILJIN composite film were also the stud pin–film exfoliation mode, and the measurement values were about 1300–2800 N cm^{-2} for the high-phosphorus-content Ni–P alloy/MWCNT composite films and 2200 N cm^{-2} for the low-phosphorus-content Ni–P alloy/ILJIN composite film. Therefore, the adhesion strengths of the high-phosphorus-content Ni–P alloy/MWCNT composite films and the low-phosphorus-content Ni–P alloy/ILJIN composite film are greater

than the measured values. No substantial difference was found between the measured values for the Ni–P alloy films and for those for the Ni–P alloy/MWCNT composite films. Thus, the adhesion strengths between the composite films and the ABS resin substrate were at least greater than 1300 N cm^{-2}. The adhesion strengths are expected to originate from the anchor effect.

Fig. 8 shows the friction coefficients of the Ni–P alloy/MWCNT composite films. For comparison, the friction coefficients of the Ni–P alloy films are also shown. The films are 3–6 μm thick, except for the Ni–P alloy/ILJIN composite films, which are 4–10 μm thick. The friction coefficients are the values at 50 cycles. No exfoliation of the film from the ABS resin substrate was observed for any sample during the friction test. This demonstrates that there is good adhesion between the composite films and the ABS resin substrates.

Fig. 9 shows SEM images of worn surfaces of the moderate-phosphorus-content Ni–P alloy/MWCNT composite films after the friction test. The scratches are not very deep and unscratched regions are visible on the surface in places. This indicates that the scratches did not reach the ABS resin substrates. This was also true for the high-phosphorus-content and low-phosphorus-content Ni–P alloy/MWCNT composite films. The Ni–P alloy/MWCNT composite films have substantially lower friction coefficients than the Ni–P alloy films in spite of the different phosphorus content of the Ni–P alloy matrix. This reduction in the friction coefficient might be due to the intrinsic lubricity of the MWCNTs. Dickrell et al. reported that the friction coefficients of vertically and transversely aligned MWCNTs are 0.795 and 0.090, respectively; they measured them under ambient conditions using a borosilicate glass pin as the counter surface [20]. Therefore, the transversely aligned MWCNTs on the composite film surface might function as a solid lubricant [21]. The Ni–P alloy/ILJIN composite films showed the highest friction coefficients in the Ni–P alloy/MWCNT composite films regardless of the phosphorus content of the Ni–P alloy matrix. Since the VGCFs, the cut VGCFs, the VGNFs, and the cut

VGNFs are graphitized MWCNTs, the crystallinity of the MWCNTs might be related to the friction coefficient of the composite films. No obvious difference was observed between the friction coefficients of the VGCFs, the cut VGCFS, the VGNFs, and the cut VGNFs. Therefore, the different lengths and diameters of the MWCNTs used in this study did not appreciably affect the friction coefficients of the composite films. Strictly speaking, the differences in the number of the MWCNTs on the film surface, the film thicknesses, and the surface roughnesses of the composite films should be taken into account; we intend to investigate this in future studies.

4. Conclusion

Electroless Ni–P alloy/MWCNT composite films containing various types of MWCNTs and having Ni–P alloy matrices with various phosphorus contents were fabricated on ABS resin substrates. The adhesion strengths of the composite films were at least greater than 1300 N cm^{-2} due to the anchor effect. The friction coefficients of the composite films were obviously lower than those of the Ni–P alloy films. Thus, the electroless CNT composite plating technique used in this study can be used to produce metal/CNT composite coatings on resins and can impart various properties of CNTs or metal/CNT composites to the resins. This technique is expected to be effective for other insulators such as ceramics.

Acknowledgements

This research was supported by Regional Innovation Cluster Program of Nagano, granted by MEXT, Japan.

References

[1] A. Oberlin, M. Endo, T. Koyama, J. Cryst. Growth 32 (1976) 335–349.

[2] S. Iijima, T. Ichihashi, Nature 363 (1993) 603–605.

[3] X.H. Chen, J.C. Peng, X.Q. Li, F.M. Deng, J.X. Wang, W.Z. Li, J. Mater. Sci. Lett. 20 (2001) 2057–2060.

[4] J. Tan, T. Yu, B. Xu, Q. Yao, Tribol. Lett. 21 (2006) 107–111.

[5] B.M. Praveen, T.V. Venkatesha, Y. Arthoba Naik, K. Prashantha, Surf. Coat. Techol. 201 (2007) 5836–5842.

[6] S. Arai, M. Endo, Electrochem. Commun. 5 (2003) 797–799.

[7] S. Arai, M. Endo, N. Kaneko, Carbon 42 (2004) 641–645.

[8] B.C. Satishkumar, E. M. Vogl, A. Govindaraj, C.N.R Rao, J. Phys. D-Appl. Phys. 29 (1996) 3173–3176.

[9] S. Arai, T. Saito, M. Endo, J. Electrochem. Soc. 157 (2010) D147–D153.

[10] W.X. Chen, J.P. Tu, H.Y. Gan, Z.D. Xu, Q.G. Wang, J.Y. Lee, Z.L. Liu, X.B. Zhang, Surf. Coat. Tech. 160 (2002) 68–73.

[11] X.H. Chen, G. Zhang, C.S. Chen, L.P. Zhou, S.L. Li, X.Q. Li, Adv. Eng. Mater. 5 (2003) 514–518.

[12] W.X. Chen, J.P. Tu, Z.D. Xu, W.L. Chen, X.B. Zhang, D.H. Cheng, Mater. Lett. 57 (2003) 1256–1260.

[13] W.X. Chen, J.P. Tu, L.Y. Wang, H.Y. Gan, Z.D. Xu, X.B. Zhang, Carbon 41 (2003) 215–222.

[14] L.Y. Wang, J.P. Tu, X.W. Chen, Y.C. Wang, X.K. Liu, C. Olk, D.H. Chang, X.B. Zhang, Wear 252 (2003) 1289–1293.

[15] Z. Yang, H. Xu, Y.L. Shi, M.K. Li, Y. Huang, H.L. Li, Mater. Res. Bull. 40 (2005) 1001–1009.

[16] X.H. Chen, C.S. Chen, H.N. Xiao, H.B. Liu, L.P. Zhou, S.L. Li, G. Zhang, Tribol. Int. 39 (2006) 22–28.

[17] S. Arai, T. Sato, M. Endo, J. Electrochem. Soc. (in press).

[18] K.C. Park, M. Fujishige, K. Takeuchi, S. Arai, S. Morimoto, M. Endo, J. Phys. Chem. Solids 69 (2008) 2481–2486.

[19] M. Endo, CHEMTEC 18 (1988) 568–576.

[20] P.L. Dickrell, S.B. Sinnott, D.W. Hahn, N.R. Raravikar, L.S. Schadler, P.M. Ajayan, W.G. Sawyer, Tribol. Lett. 28 (2005) 59–62.

[21] S. Arai, A. Fujimori, M. Murai, M. Endo, Mater. Lett. 62 (2008) 3545–3548.

Figure captions

Fig. 1 Surface SEM images of an ABS resin substrate (a) before and (b) after roughening treatment.

Fig. 2 SEM images showing growth of electroless Ni–P alloy/VGCF composite films on an ABS resin substrate: (a) before electroless deposition, (b) after 1 min, (c) after 10 min, and (d) after 30 min. The plating bath is the high-phosphorus-content bath (bath 1).

Fig. 3 Surface SEM images of various electroless Ni–P alloy/MWCNT composite films on ABS resin substrates produced from the moderate-phosphorus-content bath (bath 2) at 40 °C for 90 min: (a) Ni–P alloy film, (b) Ni–P alloy/VGCF composite film, (c) Ni–P alloy/cut VGCF composite film, (d) Ni–P alloy/VGNF composite film, (e) Ni–P alloy/cut VGNF composite film, and (f) Ni–P alloy/ILJIN composite film.

Fig. 4 Surface SEM images of electroless Ni–P alloy and Ni–P alloy/ILJIM composite films on ABS resin substrates from the low-phosphorus-content bath (bath 3) at 50 °C for 120 min: (a) Ni–P alloy film, (b) enlarged image of (a), (c) Ni–P alloy/ILJIN composite film, (d) enlarged image of (c).

Fig. 5 XRD patterns of various composite films on ABS resin substrates: (a) high-phosphorus-content Ni–P alloy/VGCF composite film, (b) moderate-phosphorus-content Ni–P alloy/ILJIN composite film, and (c) low-phosphorus-content Ni–P alloy/ILJIN composite film.

Fig. 6 Cross-sectional SEM images of (a) electroless Ni–P alloy and (b) Ni–P alloy/VGCF composite films on ABS resin substrates for the moderate-phosphorus-content bath (bath 2) at 40 °C for 90 min.

Fig. 7 Measured adhesion strengths of various moderate-phosphorus-content Ni–P alloy/MWCNT composite films.

Fig. 8 Comparison of friction coefficients of various Ni–P alloy/MWCNT composite films. The friction coefficients are the values at 50 cycles.

Fig. 9 SEM images of worn surface of the moderate-phosphorus-content Ni–P alloy/MWCNT composite films after the friction test: (a) Ni–P alloy, (b) Ni–P alloy/VGCF composite, (c) Ni–P alloy/cut-VGCF composite, (d) Ni–P alloy/VGNF composite, (e) Ni–P alloy/cut-VGNF composite, and (f) Ni–P alloy/ILJIN composite film.

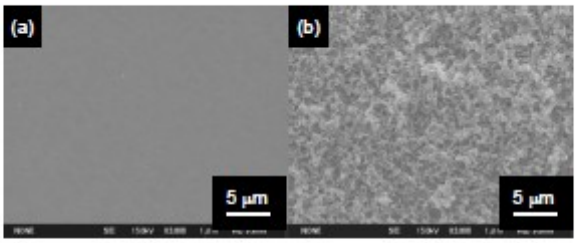

Fig. 1

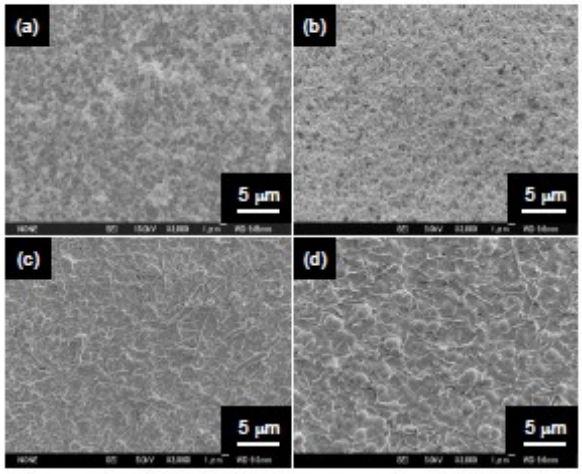

Fig. 2

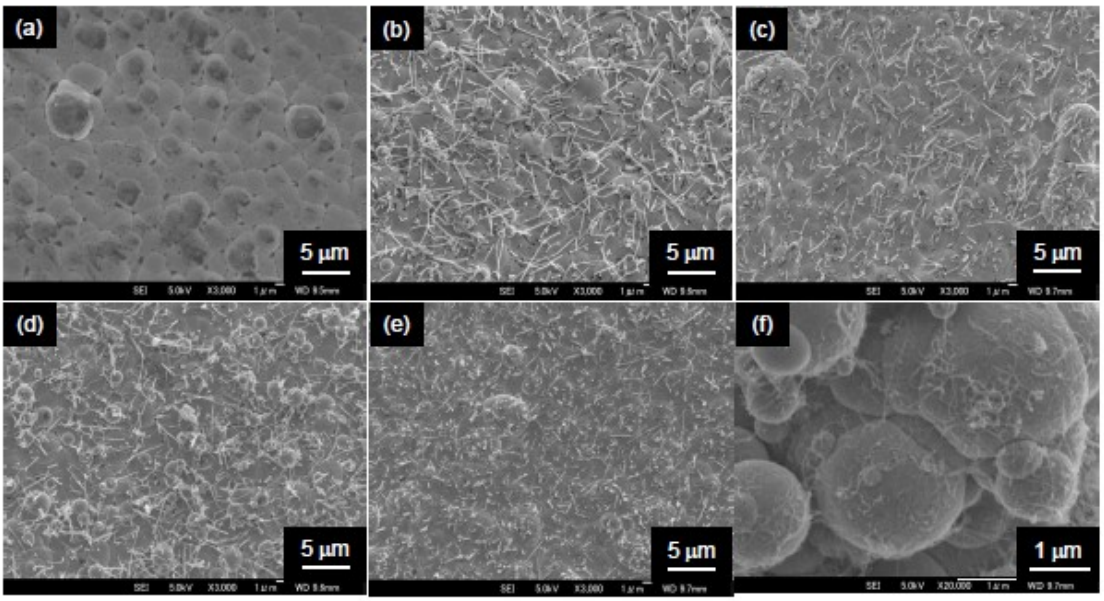

Fig. 3

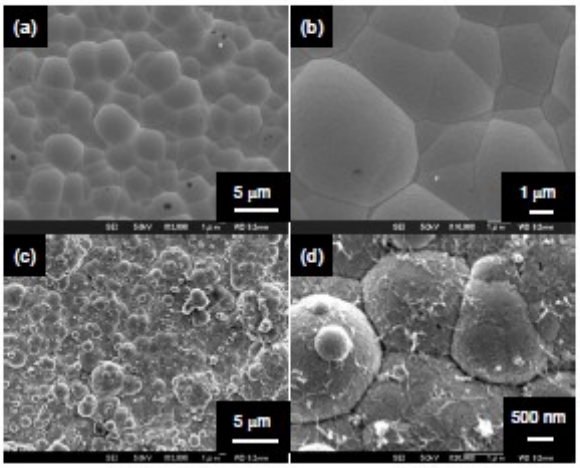

Fig. 4

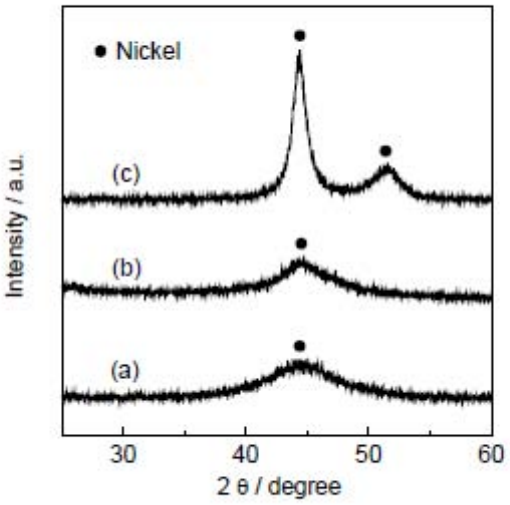

Fig. 5

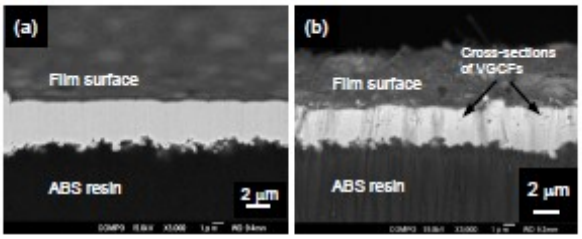
(a)
Film surface
ABS resin
2 μm
(b)
Cross-sections of VGCFs
Film surface
ABS resin
2 μm

Fig. 6

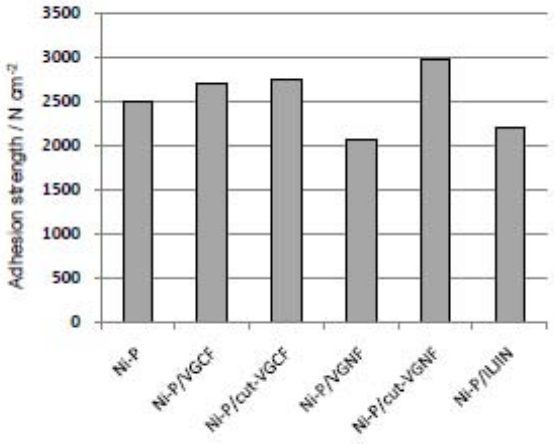
Adhesion strength / N cm-2
3500
3000
2500
2000
1500
1000
500
0
Ni-P
Ni-P/VGCF
Ni-P/cut-VGCF
Ni-P/VGNF
Ni-P/cut-VGNF
Ni-P/UIN

Fig. 7

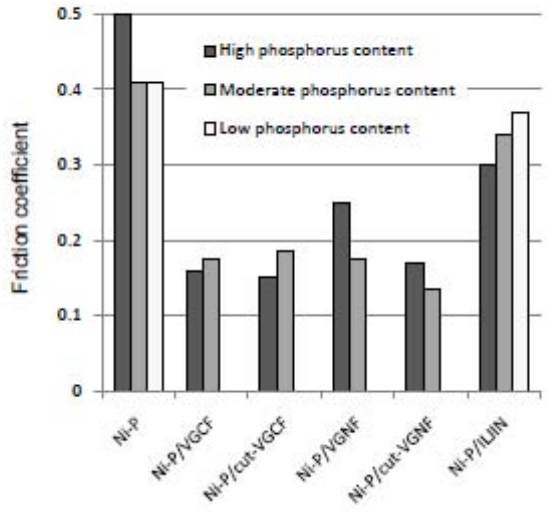
0.5
0.4
0.3
0.2
0.1
0
Friction coefficient
High phosphorus content
Moderate phosphorus content
Low phosphorus content
Ni-P
Ni-P/VGCF
Ni-P/cut-VGCF
Ni-P/VGNF
Ni-P/cut-VGNF
Ni-P/LIIN

Fig. 8

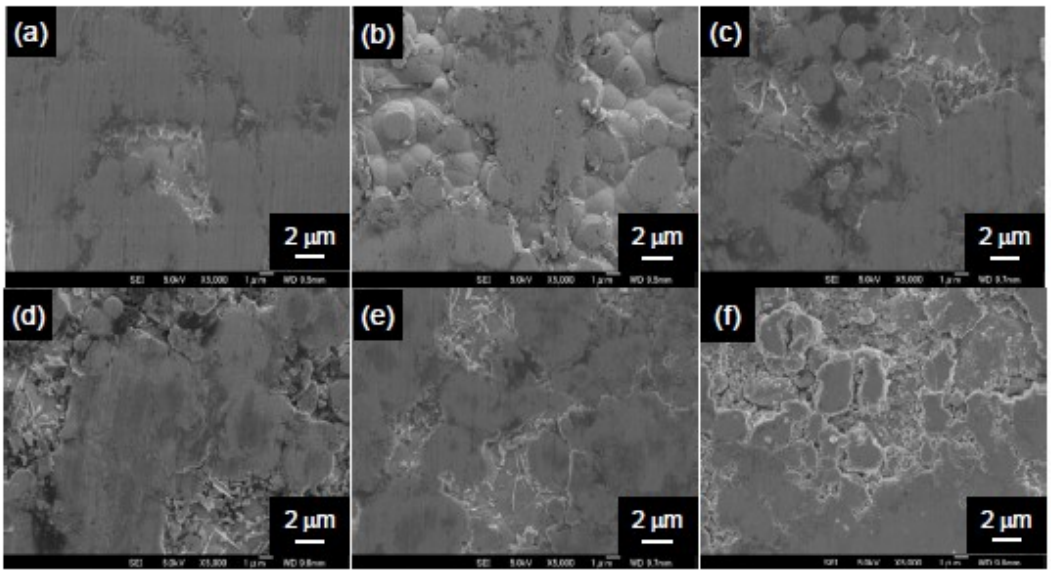

Fig. 9

Research Highlights

· Ni-P alloy/MWCNT composite films were fabricated on an ABS resin using an electroless plating technique.

· Adhesion strengths of the Ni-P alloy/MWCNT composite films were as high as the Ni-P alloy films.

· Friction coefficients of the Ni-P alloy/MWCNT composite films were lower than those of the Ni-P alloy films.